Spin Transition in the Cu(hfac)$_2$ Complex with (4-Ethylpyridin-3-yl)-Substituted Nitronyl Nitroxide Caused by the "Asymmetric" Structural Rearrangement of Exchange Clusters in the Heterospin Molecule

Natalia Artiukhova [1,2,*] , **Galina Romanenko** [1] , **Gleb Letyagin** [1,2] , **Artem Bogomyakov** [1,2] , **Sergey Veber** [1,2] , **Olga Minakova** [1,2] , **Marina Petrova** [1] , **Vitaliy Morozov** [1,2] and **Victor Ovcharenko** [1]

[1] International Tomography Center, SB RAS, Institutskaya Str., 3A, Novosibirsk 630090, Russia; romanenko@tomo.nsc.ru (G.R.); gl@tomo.nsc.ru (G.L.); bus@tomo.nsc.ru (A.B.); sergey.veber@tomo.nsc.ru (S.V.); o.minakova@g.nsu.ru (O.M.); petrovamv@tomo.nsc.ru (M.P.); moroz@tomo.nsc.ru (V.M.); Victor.Ovcharenko@tomo.nsc.ru (V.O.)

[2] Novosibirsk State University, Pirogova St., 1, Novosibirsk 630090, Russia

[*] Correspondence: natalya.artyukhova@tomo.nsc.ru

check for updates

Abstract: Methods for the synthesis of binuclear [Cu(hfac)$_2$L^{Et}]$_2$ and tetranuclear [[Cu(hfac)$_2$]$_4$(L^{Et})$_2$] heterospin compounds based on copper hexafluoroacetylacetonate [Cu(hfac)$_2$] and 2-(4-ethylpyridin-3-yl)-4,5-bis(spirocyclopentyl)-4,5-dihydro-1*H*-imidazole-3-oxide-1-oxyl (L^{Et}), were developed. The crystals of the complexes are elastic and do not crash during repeated cooling–heating cycles. It was found that a singlet–triplet conversion occurred in all of the {Cu(II)–O•–N<} exchange clusters in the molecules of the binuclear [Cu(hfac)$_2$L^{Et}]$_2$ which led to spin coupling with cooling. The transition occurred in a wide temperature range with a maximum gradient $\Delta\chi$T at ≈180 K. The structural transformation of the crystals takes place at T < 200 K and is accompanied by the lowering of symmetry from monoclinic to triclinic, twinning, and a considerable shortening of the Cu–O$_{NO}$ distance (2.19 and 1.97 Å at 295 and 50 K, respectively). For the tetranuclear [[Cu(hfac)$_2$]$_4$(L^{Et})$_2$], two structural transitions were recorded (at ≈154 K and ≈118 K), which led to a considerable change in the spatial position of the Et substituent in the nitronyl nitroxyl fragment. The low-temperature process was accompanied by a spin transition recorded as a hysteresis loop on the χT(T) curve during the repeated cooling–heating cycles (T$\frac{1}{2}$↑ = 122 K, T$\frac{1}{2}$↓ = 115 K). This transition is unusual because it causes spin coupling in half of all of the {>N–•O–Cu^{2+}} terminal exchange clusters, leading to spin compensation for only two paramagnetic centers of the six centers in the molecule.

Keywords: spin crossover; Cu(II) complexes; nitroxides; phase transitions; magnetostructural correlations

1. Introduction

Solid phases of heterospin complexes based on copper hexafluoroacetylacetonate [Cu(hfac)$_2$] with nitronylnitroxide radicals are of interest because they can undergo structural transformations accompanied by spin transitions induced by external effects [1]. Since the classic spin crossover is impossible in Cu(II) complexes with diamagnetic ligands, including the diamagnetic structural analogs of nitroxides [2], an essential condition for this effect is the coordination of an additional paramagnetic center, that is, the formation of at least a two-center exchange cluster [3]. A spin-crossover-like

phenomenon is observed when the external effect changes the mutual orientation of the paramagnetic centers and consequently the character of interaction of odd electrons. The thermally induced change in the distances between the paramagnetic centers in the {>N–•O–Cu(II)} or {>N–•O–Cu(II) –O•–N<} exchange clusters generally leads to an abrupt change in the energy and/or sign of the exchange interaction, which just gives rise to an anomaly on the curve of the temperature dependence of the magnetic susceptibility $\chi T(T)$.

Pyridyl-substituted nitronyl and imino nitroxides (Figure 1) were the first stable nitroxides for which spin transitions were recorded in their heterospin Cu(hfac)$_2$ complexes [4–8]. These transitions are generally reversible and often occur without destruction of the crystal (Single Crystal to Single Crystal transformations), due to which it is possible to trace the temperature dynamics of the structure and compare the structural features of the high- and low-temperature phases with the magnetic properties of the compound [9–21]. In the majority of these heterospin compounds, the magnetic anomalies are caused by strong antiferromagnetic exchange interactions in the {>N–•O–Cu(II)} exchange clusters, which appear at low temperatures and lead to full compensation of spins.

R = H (L^{H*}), Me (L^{Me*})   R = H (L^{H}), Me (L^{Me}), Et (L^{Et})

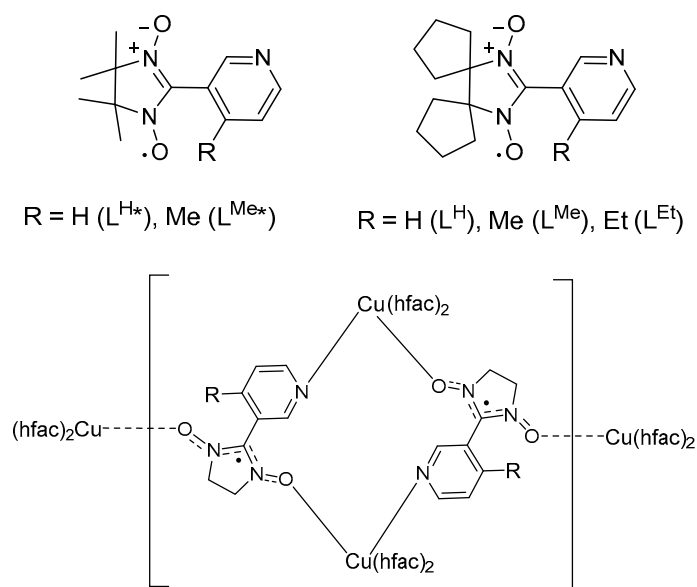**Figure 1.** L^{R} and L^{R*} radicals; structure of the [[Cu(hfac)$_2$]$_4$(L^{R})$_2$] tetranuclear complex. The fragment in square brackets is the [Cu(hfac)$_2$L]$_2$ binuclear fragment.

Earlier, it was shown that Cu(hfac)$_2$ forms binuclear and tetranuclear complexes with both L^{R*} and L^{R} (Figure 1); it also forms chain polymers {[[Cu(hfac)$_2$]$_2$L$_2$][Cu(hfac)$_2$]}$_\infty$, in which the binuclear fragments are linked into chains via additional Cu(hfac)$_2$ fragments. The spin transitions were recorded for [Cu(hfac)$_2$L^{H}]$_2$ [18], [Cu(hfac)$_2$L^{Me}]$_2$•Solv (Solv = n-C$_6$H$_{14}$, n-C$_{10}$H$_{22}$, n-C$_{16}$H$_{34}$) [9], [[Cu(hfac)$_2$]$_4$(L^{H})$_2$] [18], and [[Cu(hfac)$_2$]$_4$(L^{H*})$_2$] complexes [4,16]. We synthesized the binuclear [Cu(hfac)$_2$L^{Et}]$_2$ and tetranuclear [[Cu(hfac)$_2$]$_4$(L^{Et})$_2$] and studied their structure and magnetic properties. The present paper reports the results of this study, namely, the spin transition found for [Cu(hfac)$_2$L^{Et}]$_2$ in a wide temperature range and an unusual spin transition for [[Cu(hfac)$_2$]$_4$(L^{Et})$_2$] that is due to the coupling of only one third of the total number of spins in the molecule.

2. Materials and Methods

2.1. Chemical Materials

Cu(hfac)$_2$ [22], 1,1'-dihydroxylamino-bis-cyclopentyl sulfate monohydrate [18], and 4-ethyl nicotinaldehyde [23] used in the present study were synthesized by the known procedures.Commercial reagents and solvents were used without any additional purification. For chromatographic procedures,

TLC plates Silica Gel 60 F_{254}, aluminum sheets (Macherey-Nagel, Düren, Germany), and silica gel "0.063–0.200 mm for column chromatography" (Merck KGaA, Darmstadt, Germany) were used. The IR spectra of the samples pelletized with KBr were recorded on a VECTOR-22 spectrometer (Bruker, Karlsruhe, Germany). The melting points were determined on a heating table (VEB kombinat Nagema, Radebeul, DDR). The microanalyses were performed on an EuroEA-3000 CHNS analyser (HEKAtech, Wegberg, Germany).

2.2. Synthesis of Compounds

2-(4-Ethylpyridin-3-yl)-4,5-bis(spirocyclopentyl)-4,5-dihydro-1*H*-imidazole-3-oxide-1-oxyl (L^{Et}). 4-Ethylnicotinaldehyde (0.135 g, 1 mmol) was added to a solution of 1,1′-dihydroxylamino biscyclopentyl sulfate monohydrate (0.3 g, 1 mmol) in H_2O (3 mL) at room temperature. The reaction mixture was stirred at 50 °C for 1 h and then kept at 4 °C for 1 day. The solution was neutralized with $NaHCO_3$ until the gas ceased to evolve. The resulting precipitate was filtered off, washed on an H_2O filter, and dried in a vacuum box. This gave 2-(4-ethylpyridin-3-yl)-4,5-bis(spirocyclopentyl)-1,3-dihydroxy-imidazoline (0.250 g) in the form of a white powder, which was then used without any additional purification.

MnO_2 (1 g) was added to a suspension of the resulting adduct in MeOH (3 mL) while cooling it on a water bath, and the mixture was stirred for 1 h. The solution was filtered, the residue washed with MeOH, and the combined filtrates were evaporated. The residue was dissolved in EtOAc and filtered through a SiO_2 layer (2 ×5 cm). The eluate was evaporated on a rotor evaporator. The product was recrystallized from the CH_2Cl_2−hexane mixture, keeping it at 4 °C. The yield of L^{Et} was 0.4 g (13%), as dark blue prismatic crystals. M.p. 90–92 °C (decomp.). IR spectrum ν/cm^{-1}: 3553, 3416, 3237, 2968, 2944, 1638, 1618, 1590, 1392, 1320, 1177, 1131, 1032, 953, 844, 623, 481. Found (%): C, 68.7; H, 7.5; N, 13.5. $C_{18}H_{24}N_3O_2$. Calculated (%): C, 68.8; H, 7.7; N, 13.4.

$[Cu(hfac)_2L^{Et}]_2$. A mixture of $Cu(hfac)_2$ (0.048 g, 0.1 mmol) and L^{Et} (0.030 g, 0.1 mmol) was dissolved in acetone (1 mL). Then, hexane (4 mL) was added and the solution was kept in a refrigerator at 4 °C for 1 day. The resulting brown prismatic crystals were filtered off, washed with cold hexane, and dried in air. Yield 56 mg (72%). Found (%):C, 42.7; H, 3.2; N, 5.4; F, 28.6. $C_{56}H_{52}Cu_4F_{24}N_6O_{12}$. Calculated (%): C, 42.5; H, 3.3; N, 5.3; F, 28.8.

$[[Cu(hfac)_2]_4(L^{Et})_2]$. A mixture of $Cu(hfac)_2$ (0.076 g, 0.160 mmol) and L^{Et} (0.024 g, 0.08 mmol) was dissolved in CH_2Cl_2 (1 mL). Then, hexane (3 mL) was added and the solution was kept in an open vessel at 4 °C for 1 day. The brownish red crystalline precipitate in the form of square prisms was filtered off, washed with cold hexane, and dried in air. Yield 68 mg (68%). Found (%): C, 36.0; H, 2.2; N, 3.2; F, 36.1. $C_{76}H_{56}Cu_4F_{48}N_6O_{20}$. Calculated (%): C, 36.0; H, 2.2; N, 3.3; F, 35.9.

2.3. Magnetic Measurements

The magnetic susceptibility of the polycrystalline samples was measured on a MPMSXL SQUID magnetometer (Quantum Design, San Diego, CA, USA) in the temperature range 2−360 K in a magnetic field of up to 5 kOe. The paramagnetic components of the magnetic susceptibility χ were determined with allowance for the diamagnetic contribution evaluated from the Pascal constants. The magnetic properties were analyzed using spin-Hamiltonian in general form of H = −2$\sum J_{ij}S_iS_j$.

2.4. Crystal Structure Determinations

The arrays of reflections from single crystals were collected on Bruker (Bruker AXS GmbH, Karlsruhe, Germany) AXS-Smart Apex II (with a Helix low-temperature accessory, Oxford Cryosystems, Oxford, United Kingdom) and Apex Duo diffractometers (the absorption was included using the SADABS, version 2.10 program, Bruker AXS Inc, Karlsruhe, Germany.). The structures were solved by direct methods and refined by the full-matrix least-squares method in an anisotropic approximation for all non-hydrogen atoms. The positions of H atoms were calculated geometrically and refined in the riding model. All calculations on structure solution and refinement were performed with

SHELXL-2014/6 and SHELXL-2017/1 programs (Shelx, Göttingen, Germany) [24]. The selected bond lengths and crystal data for the compounds are listed in Tables S1 and S2, Supplementary Materials. Full information on the structures was deposited at CCDC (1907461-1907475) and can be requested at the site www/ccdc.cam.ac.uk/data_request/cif.

2.5. IR-Spectrum Experiments

The spectra were recorded over the range of $4000-700$ cm^{-1} using a HYPERION 2000 IR microscope (Bruker Optics, Ettlingen, Germany) equipped with a D316 MCT detector and coupled to a Bruker Vertex 80v FTIR spectrometer (Bruker Optics, Ettlingen, Germany). The spectral resolution was 1 cm^{-1}. A Linkam FTIR600 sample stage (Linkam Scientific Instruments, Surrey, United Kingdom) equipped with BaF$_2$ windows was used to control the temperature of the single crystal. The variable temperature FTIR (VT-FTIR) spectra of a thin single crystal of [[Cu(hfac)$_2$]$_4$(L^{Et})$_2$] were recorded in the mid-IR range at $80-274$ K at a step of 2 K. The probing area of the crystal was$\approx$0.2$\times$0.2 mm^2, which was slightly smaller than the crystal size.

2.6. Density Functional Theory (DFT) Calculations

The quantum-chemical calculations were performed in the Quantum Espresso 5.3 program package (MaX Centre of Excellence, Modena, Italy) for DFT band structure calculations in the plane wave basis by the pseudopotential method. Ultrasoft pseudopotentials with nonlinear core corrections (NLCC) and the Perdew–Burke–Ernzerhof (PBE) exchange correlation potential were used [25]. The cut off energy for the expansion of the electronic wave functions in plane waves was taken to be 35 Ry; for the charge density, the cutoff energy was 280 Ry. When integrating in the reciprocal space, we used $2 \times 2 \times 2$ k-points in the Monkhorst–Pack grid [26] in the first Brillouin zone; the Gaussian broadening was chosen to be 0.136 eV. The Hubbard corrections on the copper and oxygen atoms were applied within the framework of the GGA+U scheme with the parameters Ud(Cu) = 9.8 eV and Up(O) = 5.0 eV, respectively [27,28]. In the band DFT approach, combined with the conventional BS method to obtain exchange integrals, we calculated the set of unit cell energies for a complete number of spin polarization states of the crystal unit cell. Such an approach allows one to cover the entire net of exchange interactions of the system under study, including both the exchange couplings between the spins inside the unit cell and the exchange couplings involving spins from adjacent unit cells. Then, we mapped the selected spin Hamiltonian (the form of spin Hamiltonians are discussed in Sections 3.6 and 3.7) onto the set of energy levels obtained above. Solving the resulting system of linear equations was the final step to find the desired set of exchange integrals, characterizing the spin Hamiltonian. A comparison of the theoretical and experimental χT(T) dependences shows in all cases that the calculated exchange integrals are slightly exaggerated (approximately twofold) because of the exaggerated spin density delocalization in the DFT calculation.

3. Results

3.1. Synthesis of L^{Et}

Nitronylnitroxide L^{Et} was prepared by condensation of 4-ethylnicotinaldehyde with 1,1'-dihydroxylamino biscyclopentyl sulfate monohydrate followed by the oxidation of the resulting adduct with MnO$_2$ in EtOH (Scheme 1). The L^{Et} single crystals were grown from a CH$_2$Cl$_2$– hexane mixture.
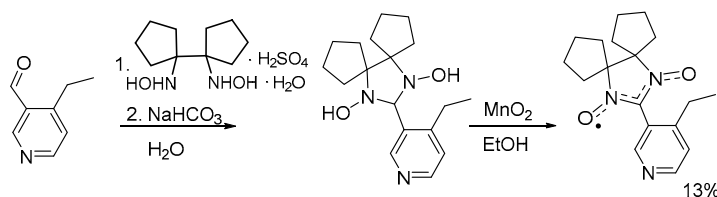
Scheme 1. Synthesis of L^{Et}.

3.2. Magnetic and X-Ray Investigations for L^{Et}

The XRD study showed that in the L^{Et} molecule, the angle between the planes of the pyridine ring and the O•–N–C=N→O fragment of the 2-imidazoline ring (∠Py–CN$_2$O$_2$) is 71.3°, and the ethyl group is almost perpendicular to the pyridine ring (Figure 2): the angle between the plane of the pyridine ring and the ethyl group (∠Py–Et) is 84.7°. The bond lengths in the N–O groups are 1.288(6) and 1.268(6) Å; the shortest distances between the paramagnetic centers in the structure exceed 4.5 Å. This agrees with χT of 0.336 K·cm^3/mol, which is almost constant at 30–300 K and close to the theoretical pure spin value of 0.375 K·cm^3/mol for one paramagnetic center with spin S = $\frac{1}{2}$ at g = 2. Antiferromagnetic exchange interactions between spins of the L^{Et} molecules are negligibly small and cause small decreasing of χT only below 20 K. The exchange coupling parameter *J* may be estimated as –1.37 cm^{-1}, using a dimer model (spin Hamiltonian $H = -2J \cdot S_1 S_2$) for the analysis of the χT(*T*) dependence (Figure 2).
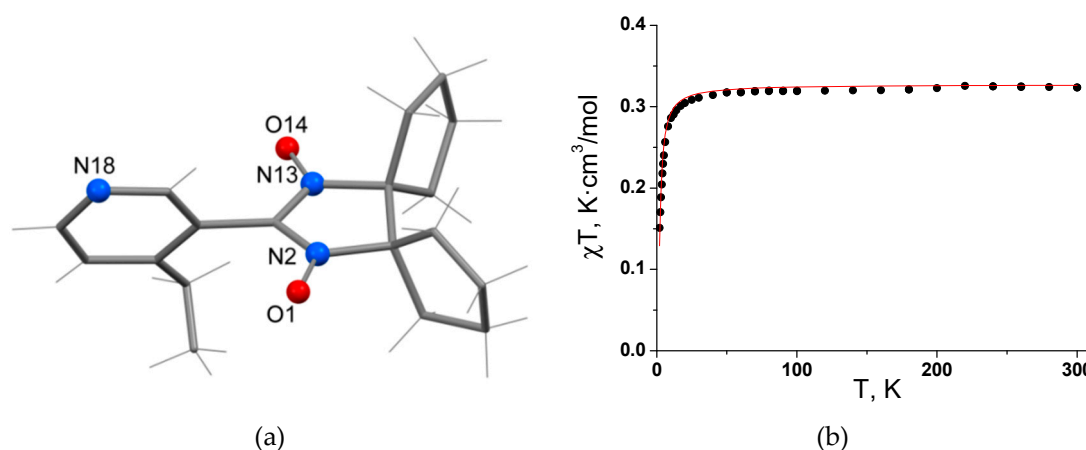

(a)　　　　　　　　　　　　　　　　　　(b)

Figure 2. Structure of L^{Et}(**a**) and temperature dependence of χT for L^{Et}(**b**).

Variation of the Cu(hfac)$_2$/L^{Et} ratio allowed us to obtain two heterospin complexes: binuclear [Cu(hfac)$_2$L^{Et}]$_2$ and tetranuclear [[Cu(hfac)$_2$]$_4$(L^{Et})$_2$], whose solid phases exhibit thermally induced spin transitions, as shown below.

3.3. Magnetic and X-Ray Investigations for [Cu(hfac)$_2$L^{Et}]$_2$

The binuclear [Cu(hfac)$_2$L^{Et}]$_2$ complex is formed by the centrosymmetric molecules (Figure 3), and the statistically averaged environment of the Cu atom at room temperature can be described as a flattened octahedron. In the octahedron, the axial positions are occupied by the pyridine N(18R) atom (1.996(2) Å) and one of the O$_{hfac}$ atoms (O2) (1.965(2) Å), whereas the O(14R) atom of the NO group (2.193(2) Å) and the other three O$_{hfac}$ atoms (2.074(2), 2.105(2), and 2.204(4) Å, Table 1) lie in the equatorial plane. When the crystal is cooled to 240 K, the Cu–O distances in the equatorial plane in the coordination unit become almost equal (2.122(4)–2.152(4) Å), which actually reflects that approximately half of all molecules have the configuration of the high-temperature phase, and the other half have the configuration of the low-temperature phase. Below 200 K, the crystal symmetry lowers from monoclinic to triclinic (see Table S1, Supplementary Materials), and the twinning effect takes place. At 50 K, the structure contains two centrosymmetric crystallographically independent molecules,

in which Cu is surrounded by an elongated octahedron with axial distances of 2.270(10)–2.338(10) Å; equatorial Cu−N distances of 1.940(11) and 1.977(10); Cu−O_{NO} 1.963(9) and 1.979(8) Å; Cu−O_{hfac} 1.944(9), 1.987(9), 1.961(9), and 2.035(9) Å for Cu1 and Cu2, respectively (Table 1).
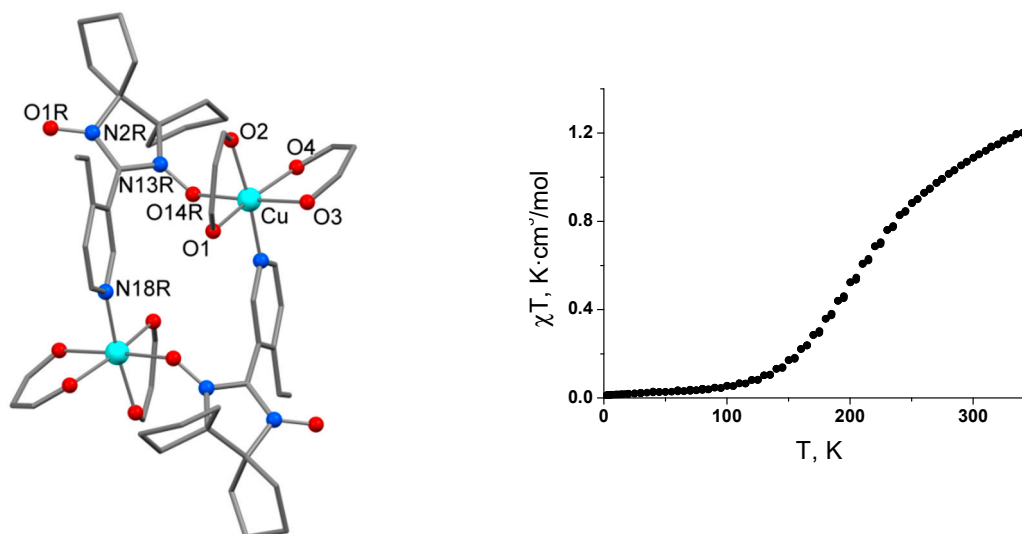

Figure 3. Molecular structure and temperature dependence of χT for $[Cu(hfac)_2L^{Et}]_2$ (H, CF_3 are omitted for clarity).

Table 1. Selected bond lengths (Å) and angles (°) in $[Cu(hfac)_2L^{Et}]_2$.

T (K)	295	240	200	50	
Cu−O_{NO}	2.193(2)	2.128(2)	2.062(5)	1.963(9)	1.979(8)
∠CuO_RN	127.8(2)	126.53(2)	126.2(4)	122.0(7)	124.9(7)
Cu−O_{hfac}	1.965(2),	1.951(3),	1.921(5),	1.944(9),	1.961(9),
	2.074(2)	2.123(3)	2.056(8)	1.987(9)	2.035(9)
	2.105(2),	2.122(4),	2.182(7),	2.302(10),	2.270(10),
	2.204(4)	2.152(3)	2.217(6)	2.338(10)	2.279(10)
Cu−N	1.996(2)	1.989(3)	1.991(6)	1.940(11)	1.977(10)
∠CN_2O_2−Py	54.7	53.8	53.0	50.1	53.6
∠Py−Et	6.7(5)	9.8(5)	7(2)	16(1)	12(2)

In $[Cu(hfac)_2L^{Et}]_2$, the interplanar angle ∠Py-CN_2O_2 is considerably smaller ($\approx 52.0°$) than in free L^{Et}, and the ethyl group lies in the plane of the pyridine ring (Table 1).

For $[Cu(hfac)_2L^{Et}]_2$, χT is 1.214 K·cm^3/mol at 315 K, which is lower than the theoretical pure spin value of 1.50 K·cm^3/mol for four paramagnetic centers with $S = \frac{1}{2}$ and $g = 2$. When the compound is cooled, χT smoothly decreases to ≈ 0.01 K·cm^3/mol, indicating that the spins almost completely vanish in the system, that is the result of the strong antiferromagnetic exchange interactions, which is typical for the equatorial coordination of the O•−N< group in Cu(II) complexes [3,5]. The character of the $\chi T(T)$ dependence is consistent with the XRD data on the shortening of the Cu−O_{NO} distances with lowering temperature (Table 1).

3.4. X-Ray Investigations for$[[Cu(hfac)_2]_4(L^{Et})_2]$

The solid $[[Cu(hfac)_2]_4(L^{Et})_2]$ is formed by the tetranuclear molecules (Figure 4). The structure of their cyclic fragment (Figure 4) is similar to that of $[Cu(hfac)_2L^{Et}]_2$ (Figure 3). The difference is that all four O atoms of the bridging L^{Et} are coordinated by the Cu atoms.

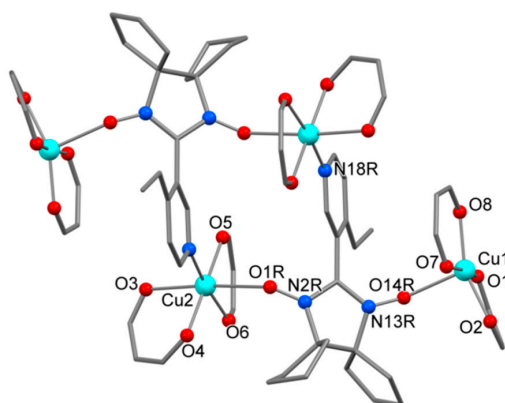**Figure 4.** Molecular structure of $[[Cu(hfac)_2]_4(L^{Et})_2]$ at 295 K and atomic numbering in its crystallographically independent part (H, CF_3 are omitted for clarity).

In the $[[Cu(hfac)_2]_4(L^{Et})_2]$ molecule, the Cu1 atoms is in a square pyramid environment formed by the O_{NO} atom lying at the apex (Cu1−O14R 2.332(2) Å) and four O_{hfac} atoms (Cu−O_{hfac} 1.915(4)−1.930(4) Å) lying at the base (Figure 4). For Cu1, the degree of distortion τ of the coordination polyhedron of the Cu atom ($\tau = 1$ for the trigonal bipyramid and 0 for the square pyramid) is 0.0603 [29]. The O_{NO} and O_{hfac} atoms lie on the elongated axis of the square bipyramid at the intracyclic Cu2 atom (Cu2−O1R 2.553(4) Å and Cu2−O3 2.285(4) Å). The interplanar angles ∠Py−CN_2O_2 and ∠Py−Et are 56.3 and 16.2°, respectively. When the crystal was cooled from 295 to 154 K, the distances in the coordination units slightly shortened (Table 2), and the angle ∠Py−Et markedly increased, from 16.2 to 36.5°. When the sample was cooled by another 4 K (i.e., to 150 K), the structure transformed in a nontrivial way: the b unit cell parameter increased three fold, and so did the crystallographically independent part, which now contained half of the centrosymmetric molecule with the Cu5 and Cu6 atoms and the complete molecule with the Cu1–Cu4 atoms (Figure 5a). The square pyramidal surrounding of the terminal Cu atoms also became much more distorted: the τ parameter increased to 0.228–0.266 (Table 2). The ∠Py−Et angle increased to 41.6° in the centrosymmetric molecule and to 53.2 and 56.3° in the non-centrosymmetric one. In the latter (the molecule in the right part of Figure 5a), the Et groups, magenta-colored in the figure, are orientated in the same direction relative to the $\{Cu_2(O_{NO})_2\}$ square plane in such a way that the terminal atom of the group is directed toward the terminal $Cu(hfac)_2$ fragment in one group and toward the plane of the hfac ligand from the cyclic dimer in the other.

Table 2. Selected bond lengths and angles in the $[[Cu(hfac)_2]_4(L^{Et})_2]$ molecules (* – after heating from 50 K).

| T, K	295	240	200	154	150	100	50	240 *
Cu−O_R (inn.)	2.553(4)	2.498(2)	2.497(2)	2.480(3)	2.526(2), 2.413(2), 2.490(2)	2.428(3), 2.424(3)	2.406(3), 2.425(3)	2.511(3)
Cu−O_R (term.)	2.276(4)	2.287(2)	2.287(2)	2.285(4)	2.308(2), 2.290(2), 2.290(2)	1.954(3), 2.281(3)	1.961(3), 2.270(3)	2.276(3)
τ	0.060	0.045	0.04650	0.042	0.228, 0.266, 0.239	0.375, 0.259	0.346, 0.253	0.263
Cu−N	1.998(4)	2.016(2)	2.016(2)	2.009(4)	2.008(3), 2.018(3), 2.016(3)	2.015(4), 2.017(4)	2.022(4), 2.021(4)	2.005(3)
∠CN_2O_2−Py	56.3	56.7	56.7	57.0	53.5, 54.7, 60.3	54.9, 57.0	54.4, 56.6	56.2
∠Py−Et	16.2	24.3	24.3	36.5	53.2, 41.6, 56.3	60.7, 63.6	61.1, 63.4	19.4

(a)

(b)   (c)
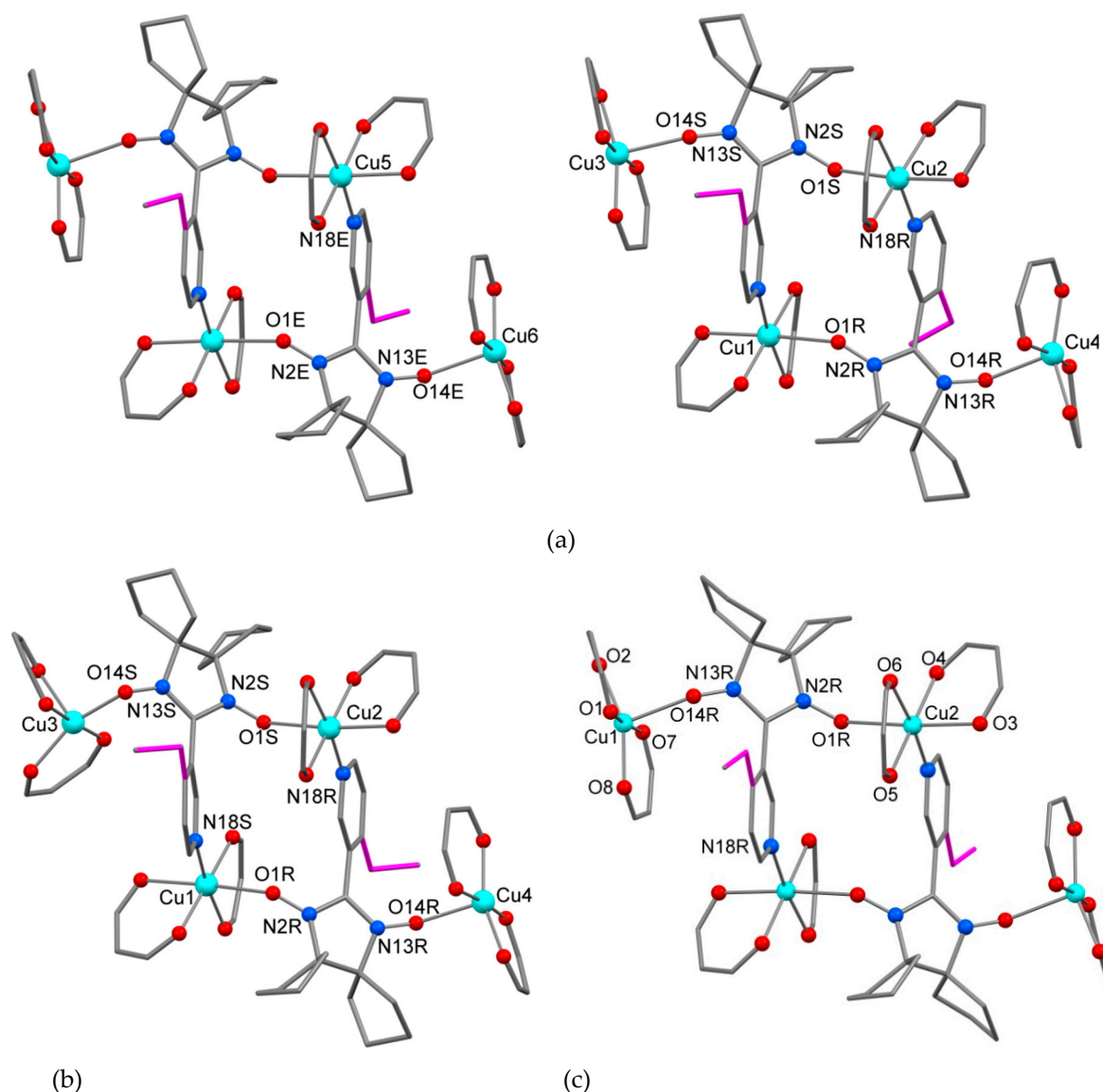
Figure 5. [[Cu(hfac)$_2$]$_4$(L^{Et})$_2$]: molecular structure and atomic numbering in the crystallographically independent part (**a**) at 150 K, (**b**) at 100 K, and (**c**) after return to 240 K; the Et groups are magenta-colored (H and CF$_3$ are omitted for clarity).

When the crystal was further cooled to 100 K, the *b* parameter became close to the initial value, whereas the *a* parameter doubled. The crystallographically independent part of the structure at 100 K was a complete [[Cu(hfac)$_2$]$_4$(L^{Et})$_2$] molecule. According to Figure 5b, the Et groups were again orientated in different directions (the ∠Py−Et angle is 60.7 and 63.3°). The surrounding of the terminal Cu3 and Cu4 atoms changed dramatically. For Cu3, the square pyramidal environment was preserved, with the O$_{NO}$ atom at the apex (Cu−O 2.281(3) Å). For Cu4, however, the apex of the square pyramid was occupied by the O$_{hfac}$ atom (Cu−O 2.158(3) Å), while O$_{NO}$ shifted to the base (Cu−O$_{NO}$ 1.954(3), Cu−O$_{hfac}$ 1.918(4)–1.957(3) Å) and τ increased to 0.375 (Table 2). Further cooling of the crystal to 50 K did not reveal any significant changes in the structure. After the crystal was further heated to 240 K, the high-temperature phase was recovered (Table S2 (Supplementary Materials) and Table 2, Figure 5c) except that the square pyramidal environment of the terminal Cu atom remained rather strongly distorted: τ = 0.263, whereas its initial value was 0.045.

3.5. IR Spectroscopy of $[[Cu(hfac)_2]_4(L^{Et})_2]$

Earlier, VT-FTIR was shown to be highly sensitive to the temperature-induced structural transitions in copper–nitroxide complexes [30]. Figure 6a presents the temperature dependence of a fragment of the absorption spectrum of the $[[Cu(hfac)_2]_4(L^{Et})_2]$ single crystal at 80–274 K and shows the regions for which integration was performed and the temperature dependences calculated (Figure 6b). When the crystal was cooled from 274 to 158 K, the intensity of the IR absorption bands changed insignificantly and monotonically. Below 158 K, some of the IR absorption lines significantly changed their intensity and position, confirming the XRD data considered above. These changes were most dramatic at energies of 849–841 cm^{-1}, at which a new absorption band centered at 847 cm^{-1} appeared. Further cooling to 80 K revealed only one more structural transition, which strongly affected all the absorption bands being considered (Figure 6b). The temperature of this transition agreed well with the temperature of the magnetic transition (Figure 6c) and also demonstrated a hysteresis of a few K. Thus, VT-FTIR of $[[Cu(hfac)_2]_4(L^{Et})_2]$ reliably confirmed both transitions observed by XRD and SQUID.
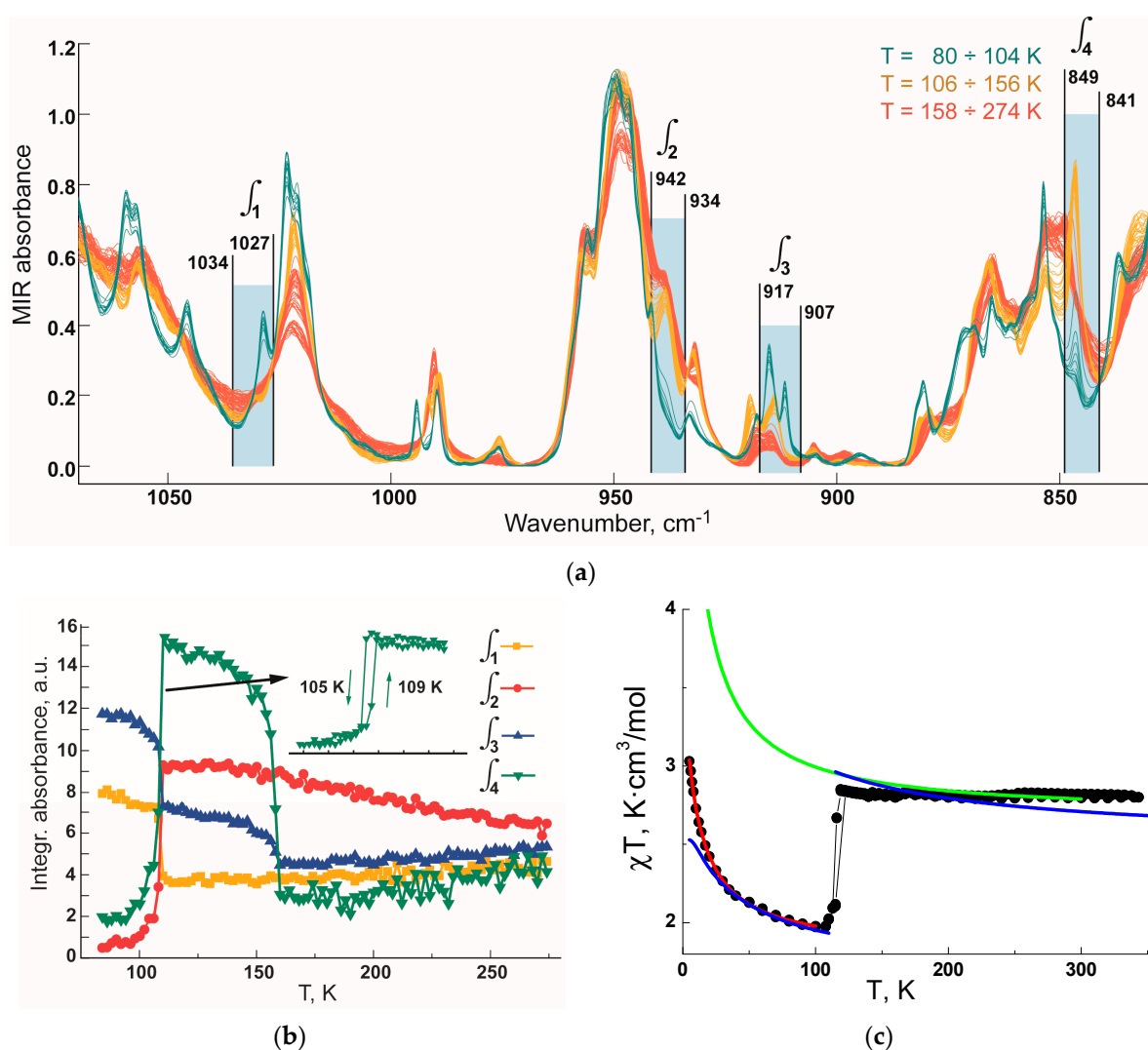

Figure 6. (**a**) Variable temperature FTIR (VT-FTIR) spectra of the $[[Cu(hfac)_2]_4(L^{Et})_2]$ single crystal in the mid-IR range measured at different temperatures; (**b**) temperature dependencies of the integrated intensity of the absorption bands in the ranges marked in (**a**); (**c**) dependence $\chi T(T)$. The solid lines on the $\chi T(T)$ dependence are the theoretical curves (see the text for explanations).

3.6. Magnetic Investigations for [[Cu(hfac)$_2$]$_4$(L^{Et})$_2$]

Figure 6c shows the temperature dependence of χT for [[Cu(hfac)$_2$]$_4$(L^{Et})$_2$]. The χT value does not change in the range of 122–345 K and equals 2.80 K cm^3/mol, which is slightly higher than the theoretical pure spin value of 2.25 K·cm^3/mol for six non-interacting paramagnetic centers with spin S = $\frac{1}{2}$ and g = 2. The exaggerated χT value is caused by g$_{Cu}$ > 2. Below 122 K, χT drastically decreases, reaching 1.97 K·cm^3/mol at 107 K, which agrees with the theoretical value for four non-interacting unpaired electrons, and then increases to 3.03 K cm^3/mol at 5 K. As mentioned above, at 150–100 K the environment of one of the terminal atoms in the structure transforms with a drastic shortening of the Cu–O$_{NO}$ distance, giving rise to strong antiferromagnetic exchange interactions in the >N–•O–Cu^{2+} exchange clusters, which lead to complete compensation of their spins. When the sample is further cooled, χT increases, which confirms the intramolecular ferromagnetic exchange between the remaining paramagnetic centers. The χT(T) dependence in the range of 5–100 K was analyzed in terms of the following spin Hamiltonian:

$$H= -2J_1 \cdot S_{Cu3}S_{R1} - 2J_2 \cdot (S_{Cu2}S_{R1} + S_{Cu1}S_{R2}) - 2J_3 \cdot (S_{Cu2}S_{R2} + S_{Cu1}S_{R1}) - 2J_4 \cdot S_{Cu4}S_{R2} \qquad (1)$$

using the PHI program [31]. The optimum values of the J_1, J_2, J_3, and J_4 parameters are 15.3, 8.75, 2.12, and –461 cm^{-1}, respectively, at g$_{Cu}$ = 2.27 and g$_R$ = 2.0 (fixed) (Figure 6c, red line). If we set that $J_4 = J_1 = 15.3$ cm^{-1}, then the theoretical curve describes well the experimental data in the high-temperature range of 150–300 K (Figure 6c, green line).

3.7. Quantum-Chemical Calculations for [[Cu(hfac)$_2$]$_4$(L^{Et})$_2$]

The quantum-chemical calculations of the exchange interaction parameters for [[Cu(hfac)$_2$]$_4$(L^{Et})$_2$] were performed using the following spin Hamiltonian:

$$H = -2J_1 \cdot S_{Cu3}S_{R1} - 2J_{21} \cdot S_{Cu2}S_{R1} - 2J_{22} \cdot S_{Cu1}S_{R2} - 2J_4 \, S_{Cu4}S_{R2} \qquad (2)$$

where S_{R1} and S_{R2} are the spins of the nitronylnitroxides lying between Cu1 and Cu3 (R1) and Cu2 and Cu4 (R2), respectively (Figure 5b). The exchange integrals of the spin Hamiltonian were calculated by the broken symmetry method [32] from the energies of the spin configurations determined by DFT quantum-chemical band structure calculations. The resulting exchange integrals are shown in Table 3.

Table 3. Exchange integrals (cm^{-1}) in the [[Cu(hfac)$_2$]$_4$(L^{Et})$_2$] molecules.

T, K	J_{21}	J_1	J_{22}	J_4
50	37.7	15.2	49.9	−719.0
100	37.7	14.9	49.0	−720.0
153	37.1	12.9	37.1	12.9
295	32.7	9.6	32.7	9.6

Our calculations confirmed the appearance of strong antiferromagnetic exchange in the terminal >N–•O–Cu^{2+} fragment when the position of the coordinated O$_{NO}$ atom changed from axial to equatorial at T < 122 K. The exchange integral calculated for this case, $J_4 = -720$ cm^{-1}, as well as the positive exchange integrals at T > 154 K, qualitatively agree with the exchange parameters obtained by fitting the experimental curve χT(T) (Figure 6c), but are slightly overestimated, what is typical for quantum-chemical calculations [33]. The temperature dependences χT(T) calculated using the exchange integrals from Table 3 are shown in Figure 6c (blue lines). At T < 100 K, the exchange integrals were used for T = 100 K; at T > 153 K, for T = 295 K, g$_{Cu}$ = 2.15, g$_R$ = 2.05. The quantum-chemical calculations also show that other exchange integrals in [[Cu(hfac)$_2$]$_4$(L^{Et})$_2$] are positive, which explains the fast growth of the χT when the temperature lowers at T < 100 K. It was also assumed that the exchange interaction between the spins of the intracyclic copper Cu1 and Cu2 ions with nitroxides R1

and R2 via the pyridine ring is small. For this reason, it was not calculated, although it can contribute to the growth of the χT to 3.03 K cm^3/mol at T < 10 K for [[Cu(hfac)$_2$]$_4$(L^{Et})$_2$].

4. Conclusions

New molecular heterospin complexes [Cu(hfac)$_2$L^{Et}]$_2$ and [[Cu(hfac)$_2$]$_4$(L^{Et})$_2$] exhibiting reversible spin transitions were obtained as a result of this study. The crystals of the complexes are mechanically stable and do not crash during the repeated cooling–heating cycles, which allowed us to study the structure of both the high- and low-temperature phases. The thermally induced structural rearrangement in the binuclear complex was accompanied by the change in its symmetry. When the tetranuclear complex was cooled, two structural phase transitions were observed, the low-temperature transition provoking the spin transition. This transition is unusual, since it causes spin coupling in half of all terminal {>N–•O–Cu^{2+}} exchange clusters, which leads to spin compensation of only two paramagnetic centers of the six centers present in the molecule. This "asymmetric" coupling of the electrons of the paramagnetic centers inside one molecule, that has not been observed earlier for multinuclear Cu(II) complexes with nitroxides [4,5,18]. This effect can evidently be responsible for the appearance of stepwise spin transitions in multinuclear compounds with several exchange clusters in the molecule. For [[Cu(hfac)$_2$]$_4$(L^{Et})$_2$] molecules, however, the transition to the low-spin state in the second terminal {>N–•O–Cu^{2+}} fragment was not recorded after the cooling to 2 K.

Supplementary Materials: The following are available online at http://www.mdpi.com/2073-4352/9/6/285/s1, Table S1: Crystallographic data and experimentdetails for [Cu(hfac)$_2$(L^{Et})]$_2$; Table S2: Crystallographic data and experiment details for [[Cu(hfac)$_2$]$_4$(L^{Et})$_2$].

References

1. Ovcharenko, V.I.; Bagryanskaya, E.G. *Spin-Crossover Materials: Properties and Applications*; Halcrow, M., Ed.; John Wiley & Sons Ltd.: Chichester, UK, 2013.
2. Tretyakov, E.V.; Tolstikov, S.E.; Suvorova, A.O.; Polushkin, A.V.; Romanenko, G.V.; Bogomyakov, A.S.; Veber, S.L.; Fedin, M.V.; Stass, D.V. Crucial role of paramagnetic ligands for magnetostructural anomalies in "breathing crystals". *Inorg. Chem.* **2012**, *51*, 9385–9394. [CrossRef] [PubMed]
3. Ovcharenko, V.I.; Romanenko, G.V.; Maryunina, K.Y.; Bogomyakov, A.S.; Gorelik, E.V. Thermally Induced Magnetic Anomalies in Solvates of the Bis(hexafluoroacetylacetonate) copper (II) Complex with Pyrazolyl-Substituted NitronylNitroxide. *Inorg. Chem.* **2008**, *47*, 9537–9552. [CrossRef]
4. Lanfranc de Panthou, F.; Belorizky, E.; Calemczuk, R.; Luneau, D.; Marcenat, C.; Ressouche, E.; Turek, P.; Rey, P. A new type of thermally-induced spin transition associated with an equatorial. dblarw. axial conversion in a copper(II)-nitroxide cluster. *J. Am. Chem. Soc.* **1995**, *117*, 11247–11253.
5. Lanfranc de Panthou, F.; Luneau, D.; Musin, R.N.; Öhrström, L.; Grand, A.; Turek, P.; Rey, P. Spin-Transition and Ferromagnetic Interactions in Copper(II) Complexes of a 3-Pyridyl-Substituted IminoNitroxide. Dependence of the Magnetic Properties upon Crystal Packing. *Inorg. Chem.* **1996**, *35*, 3484–3491. [CrossRef]
6. Rey, P.; Ovcharenko, V.I. Copper(II) Nitroxide Molecular Spin-transition Complexes. In *Magnetism: Molecules to Materials: 5 Volumes Set*; Miller, J.S., Drillon, M., Eds.; Wiley-VCH: New York, NY, USA, 2003; pp. 41–63.
7. Ovcharenko, V.I. Metal-nitroxide complexes: synthesis and Magnetostructural Correlations. In *Stable Radicals: Fundamentals and Applied Aspects of Odd-Electron Compounds*; Hicks, R., Ed.; Wiley-VCH: New York, NY, USA, 2010; pp. 461–507.

8. Halcrow, M. *Spin-Crossover Materials: Properties and Applications*; John Wiley & Sons Ltd.: Chichester, UK, 2013.

9. Tolstikov, S.E.; Artiukhova, N.A.; Romanenko, G.V.; Bogomyakov, A.S.; Zueva, E.M.; Barskaya, I.Y.; Fedin, M.V.; Maryunina, K.Y.; Tretyakov, E.V.; Sagdeev, R.Z. Heterospin complex showing spin transition at room temperature. *Polyhedron* **2015**, *100*, 132–138. [CrossRef]

10. Wang, Y.-L.; Gao, Y.-Y.; Yang, M.-F.; Gao, T.; Ma, Y.; Wang, Q.-L.; Liao, D.-Z. Four new Cu-coordination compounds based on different nitronylnitroxide radicals: Structural design and magneto-structural correlations. *Polyhedron* **2013**, *61*, 105–111. [CrossRef]

11. Yang, M.; Sun, J.; Guo, J.; Sun, G.; Li, L. Cu–Ln compounds based on nitronylnitroxide radicals: Synthesis, structure, and magnetic and fluorescence properties. *Cryst. Eng. Comm.* **2016**, *19*, 9345–9356. [CrossRef]

12. Souza, D.A.; Florencio, A.S.; Soriano, S.; Calvo, R.; Sartoris, R.P.; Carneiro, J.W.d.M.; Sangregorio, C.; Novak, M.A.; Vaz, M.G.F. New copper(II)-radical one dimensional chain: Synthesis, crystal structure, EPR, magnetic properties and DFT calculations. *Dalton Trans.* **2009**, *34*, 6816–6824. [CrossRef]

13. Souza, D.A.; Moreno, Y.; Ponzio, E.A.; Resende, J.A.; Jordao, A.K.; Cunha, A.C.; Ferreira, V.F.; Novak, M.A.; Vaz, M.G.F. Synthesis, crystal structure, magnetism and electrochemical properties of two copper(II) furoyltrifluoroacetonate complexes with nitroxide radical. *Inorg. Chim. Acta* **2011**, *370*, 469–473. [CrossRef]

14. Caneschi, A.; Ferraro, F.; Gatteschi, D.; Rey, P.; Sessoli, R. Structure and magnetic properties of a chain compound formed by copper (II) and a tridentate nitronylnitroxide radical. *Inorg. Chem.* **1991**, *30*, 3162–3166. [CrossRef]

15. Yeltsov, I.; Ovcharenko, V.; Ikorskii, V.; Romanenko, G.; Vasilevsky, S. Copper(II) Thenoyltrifluoroacetonate as Acceptor Matrix in Design of Heterospin Complexes. *Polyhedron* **2001**, *20*, 1215–1222. [CrossRef]

16. Hirel, C.; Li, L.; Brough, P.; Vostrikova, K.; Pecaut, J.; Mehdaoui, B.; Bernard, M.; Turek, P.; Rey, P. New spin-transition-like-nitroxide species. *Inorg. Chem.* **2007**, *46*, 7545–7552. [CrossRef]

17. Wang, K.-M.; Du, L.; Fang, R.-B.; Zhao, Q.-H. Synthesis and Crystal Structure of Copper(II)-Hexafluoro-Acetylacetonate Complexes with Pyridyl-Substituted Nitronyl and Imino-Nitroxide Radicals. *J. Chem. Cryst.* **2010**, *40*, 472–475. [CrossRef]

18. Artiukhova, N.A.; Maryunina, K.Y.; Fokin, S.V.; Tretyakov, E.V.; Romanenko, G.V.; Polushkin, A.V.; Bogomyakov, A.S.; Sagdeev, R.Z.; Ovcharenko, V.I. Spirocyclic Derivatives of NitronylNitroxides in the Design Of Heterospin Cu(II) Complexes Manifesting Spin Transitions. *Russ. Chem. Bull.* **2013**, *62*, 2132–2140. [CrossRef]

19. Wang, X.-F.; Licun Li, P.H.; Sutter, J.-P. [(Cu-Radical)$_2$-Ln]: Structure and Magnetic Properties of a Hetero-tri-spin Chain of Rings (Ln = Y^{III}, Gd^{III}, Tb^{III}, Dy^{III}). *Inorg. Chem.* **2015**, *54*, 9664–9669. [CrossRef]

20. Wang, X.-F.; Hu, P.; Li, Y.-G.; Li, L.-C. Construction of NitronylNitroxide-Based 3d–4f Clusters: Structure and Magnetism. *Chem. Asian J.* **2015**, *10*, 325–328. [CrossRef]

21. Artiukhova, N.A.; Romanenko, G.V.; Letyagin, G.A.; Bogomyakov, A.S.; Tolstikov, S.E.; Ovcharenko, V.I. Spin transition characteristics of molecular solvates of Cu^{II} complexes with nitroxides: Sensitivity to the packing type. *Russ. Chem. Bull* **2019**, *68*, 732–742. [CrossRef]

22. Bertrand, J.A.; Kaplan, R.I. A Study of Bis(hexafluoroacetylacetonato)copper(II). *Inorg. Chem.* **1966**, *5*, 489–491. [CrossRef]

23. Gueritte, F.; Guillou, C.; Husson, H.-P.; Kozielski, F.; Labriere, C.; Skoufias, D.; Tcherniuk, S.; Thal, C. Use of Derivatives of Indoles for the Treatment of Cancer. EP2266562A1, 29 December 2010.

24. Sheldrick, G.M. Crystal structure refinement with SHELXL. *Acta Cryst.* **2015**, *C71*, 3–8.

25. Giannozzi, P.; Baroni, S.; Bonini, N.; Calandra, M.; Car, R.; Cavazzoni, C.; Ceresoli, D.; Chiarotti, G.L.; Cococcioni, M.; Dabo, I. QUANTUM ESPRESSO: A modular and open-source software project for quantum simulations of materials. *J. Phys. Condens. Matter.* **2009**, *21*, 395502–395520. [CrossRef]

26. Monkhorst, H.J.; Pack, J.D. Special points for Brillouin-zone integrations. *Phys. Rev. B* **1976**, *13*, 5188–5192. [CrossRef]

27. Streltsov, S.V.; Petrova, M.V.; Morozov, V.A.; Romanenko, G.V.; Anisimov, V.I.; Lukzen, N.N. Interplay between lattice, orbital, and magnetic degrees of freedom in the chain-polymer Cu(II) breathing crystals. *Phys. Rev. B* **2013**, *87*, 024425–024425/6. [CrossRef]

28. Morozov, V.A.; Petrova, M.V.; Lukzen, N.N. Exchange coupling transformations in Cu (II) heterospin complexes of "breathing crystals" under structural phase transitions. *AIP Adv.* **2015**, *5*, 087161. [CrossRef]

29. Addison, A.W.; Rao, T.N.; Reedijk, J.; van Rijn, J.; Verschoor, G.C. Synthesis, structure, and spectroscopic properties of copper(II) compounds containing nitrogen–sulphur donor ligands; the crystal and molecular structure of aqua [1,7-bis(N-methylbenzimidazol-2'-yl)-2,6-dithiaheptane]copper(II) perchlorate. *J. Chem. Soc. Dalton Trans.* **1984**, *7*, 1349–1356. [CrossRef]

30. Veber, S.L.; Suturina, E.A.; Fedin, M.V.; Boldyrev, K.N.; Maryunina, K.Y.; Sagdeev, R.Z.; Ovcharenko, V.I.; Gritsan, N.P.; Bagryanskaya, E.G. FTIR study of thermally induced magnetostructural transitions in breathing crystals. *Inorg Chem.* **2015**, *54*, 3446–3455. [CrossRef]

31. Chilton, N.F.; Anderson, R.P.; Turner, L.D.; Soncini, A.; Murray, K.S. PHI: A powerful new program for the analysis of anisotropic monomeric and exchange-coupled polynuclear d- and f-block complexes. *J. Comput. Chem.* **2013**, *34*, 1164–1175. [CrossRef]

32. Yamaguchi, K.; Fukui, H.; Fueno, T. Molecular Orbital (MO) Theory for Magnetically Interacting Organic Compounds. Ab-Initio MO Calculations of the Effective Exchange Integrals For Cyclophane-Type Carbene Dimers. *Chem. Lett.* **1986**, *15*, 625–628. [CrossRef]

33. Cho, D.; Ko, K.C.; Ikabata, Y.; Wakayama, K.; Yoshikawa, T.; Nakai, H.; Lee, J.Y. Effect of Hartree-Fock exact exchange on intramolecular magnetic coupling constants of organic diradicals. *J. Chem. Phys.* **2015**, *142*, 024318. [CrossRef]